



Cite this: *Phys. Chem. Chem. Phys.*,
2017, **19**, 12749

Doped δ -bismuth oxides to investigate oxygen ion transport as a metric for condensed phase thermite ignition†

Xizheng Wang, Wenbo Zhou, Jeffery B. DeLisio, Garth C. Egan and Michael R. Zachariah *

Nanothermites offer high energy density and high burn rates, but are mechanistically only now being understood. One question of interest is how initiation occurs and how the ignition temperature is related to microscopic controlling parameters. In this study, we explored the potential role of oxygen ion transport in Bi_2O_3 as a controlling mechanism for condensed phase ignition reaction. Seven different doped δ - Bi_2O_3 were synthesized by aerosol spray pyrolysis. The ignition temperatures of Al/doped Bi_2O_3 , C/doped Bi_2O_3 and Ta/doped Bi_2O_3 were measured by temperature-jump/time-of-flight mass spectrometer coupled with a high-speed camera respectively. These results were then correlated to the corresponding oxygen ion conductivity (directly proportional to ion diffusivity) for these doped Bi_2O_3 measured by impedance spectroscopy. We find that ignition of thermite with doped Bi_2O_3 as oxidizer occurs at a critical oxygen ion conductivity ($\sim 0.06 \text{ S cm}^{-1}$) of doped Bi_2O_3 in the condensed-phase so long as the aluminum is in a molten state. These results suggest that oxygen ion transport limits the condensed state Bi_2O_3 oxidized thermite ignition. We also find that the larger oxygen vacancy concentration and the smaller metal–oxide bond energy in doped Bi_2O_3 , the lower the ignition temperature. The latter suggests that we can consider the possibility of manipulating microscopic properties within a crystal, to tune the resultant energetic properties.

Received 14th December 2016,
Accepted 28th April 2017

DOI: 10.1039/c6cp08532f

rsc.li/pccp

Introduction

The thermite reaction has historically generated interest due to its high specific energy density.¹ Compared to traditional organic based energetic materials such as TNT (trinitrotoluene) and RDX (hexogen), thermites have higher gravimetric and volumetric reaction enthalpies.² The kinetics of the reaction are known to be accelerated when the fuel and oxidizer are at the nanoscale, resulting from the increased interfacial contact and reduced characteristic diffusion length scale. Aluminum is by far the most commonly used fuel due to its high oxidation potential, ready availability and low density.^{3,4} Nano-aluminum has a native Al_2O_3 shell, which must be breached in order for the fuel and oxidizer to react. Rosenband found melting aluminum leaks through cracks resulting from the expanding outer shell of Al_2O_3 .⁵ Trunov *et al.* proposed that ignition occurs when the particle's temperature exceeds the alumina melting point.⁶ Sullivan *et al.* proposed nanothermites undergo a reactive

sintering mechanism, where initiation of the reaction occurs when condensed-phase reactants are in interfacial contact.^{7,8}

On the other hand there are many oxidizers, typically metal oxides, available to complete the redox reaction. It is the properties of the oxidizers on ignition that is very much an open question, as it is well known that reactivity and ignition behavior do not correlate well with overall reaction enthalpy. More generally, the initiation mechanism of the thermite reaction is being explored by several research groups.^{9–12} The basic questions at hand are, what species initiate the reaction, what form are they in, and how is it transported? Answering this question could lead to a better understanding on how best to choose oxidizers. Jian *et al.*¹² recently investigated whether gas phase oxygen generation from an oxidizer is an essential prerequisite to ignition under rapid heating rate conditions, and found large differences in ignition temperatures among different nanothermite formulations involving aluminum and metal oxides. For instance, many formulations (*e.g.*, Al–CuO) have ignition temperatures slightly higher than the decomposition temperatures of the oxidizers, suggesting gas-phase oxygen generation may be necessary for the ignition. However, some formulations (*e.g.*, Al– Bi_2O_3) have ignition temperatures lower than the decomposition temperatures of oxidizers, suggesting a condensed phase reaction

Department of Chemical and Biomolecular Engineering and Department of Chemistry and Biochemistry, University of Maryland, College Park, Maryland 20742, USA. E-mail: mrz@umd.edu

† Electronic supplementary information (ESI) available. See DOI: 10.1039/c6cp08532f

mechanism that is not governed by the release of gas-phase oxygen. Al–Bi₂O₃ is one of the most interesting formulations for two reasons: the ignition temperature (~630 °C) is much lower than the decomposition temperature of Bi₂O₃ (~1330 °C), which leads to ignition almost certainly through a condensed phase reaction.¹³ The other is that Bi₂O₃ has the highest known oxygen ion conductivity,¹⁴ which one might reasonably expect to be an important parameter, although it has not heretofore been explored in the thermite reaction. In a recent parallel study we employed nine lanthanum based perovskites with different Sr²⁺ doping of the A-site, and different B-site transition metals.¹⁵ The perovskites O₂ release and ignition temperatures with aluminum were measured under fast heating (>10⁵ °C s⁻¹). The results showed a linear relationship between average bond energy and electronegativity with ignition temperature. This was the first demonstration of the connection between metal–oxygen bond energy, electronegativity and ignition temperature. Furthermore it suggests that further studies of oxygen ion diffusivity in metal oxides are warranted. Ion-diffusion coefficients can be measured through a determination of mobility or more directly through an electrical measurement of ion conductivity.¹⁶ One feature of Bi₂O₃ which makes it particularly attractive for our purposes is that it is an ionic conductor, which implies that we have a direct opportunity to measure oxygen-ion conductivity, not readily available in other systems which mostly are mixed ion and electron conductors.¹⁷

While aluminum is nominally the fuel of choice, for the purposes of tweezing out mechanistic information we will also study both carbon and tantalum as fuels. Based on previous work in our group with carbon black as a fuel,¹³ the C/Bi₂O₃ system, although not violent, offers a valuable mechanistic perspective, in that the carbon nanoparticle, unlike aluminum, has no oxide shell, thus no barrier for the oxygen species migration that leads to ignition. Additionally, C will remain solid and thus not particularly mobile. Therefore, the ignition of C/Bi₂O₃ is expected to be controlled by the transport of bound oxygen from the oxidizer. Tantalum is another candidate as a high energy density fuel due to the high negative enthalpy of formation of tantalum oxide.¹⁸ Similar to aluminum, tantalum also has a surface passivating amorphous oxide shell. However, tantalum has a very high melting temperature (~3000 °C),¹⁹ which lies far above the ignition temperature. Thus we have three different fuels, one (Al) with a low melting point and a passivating oxide, one (Ta) with a high melting point and a passivating oxide and one (C) with a high melting point with no passivating oxide.

Studies on all of the aforementioned fuels with Bi₂O₃ allude to the importance of oxygen transport, which is directly related to the temperature dependent internal structure of Bi₂O₃. Pure cubic δ-Bi₂O₃'s high oxygen ion conductivity results from the large number of highly mobile oxygen vacancies, weak Bi–O bond and high polarizability of Bi³⁺ with its lone 6s² electrons. However, δ-Bi₂O₃ is less thermodynamically stable than the monoclinic α-phase below 730 °C,²⁰ but can be stabilized down to room temperature by doping with other oxides.²¹ However, due to the mismatch in ionic radii between the host and dopant cations and a related phenomenon, anion ordering, phase stabilization

lowers the oxygen ion conductivity.¹⁴ Several studies report that due to the large dopant radii and high polarizability of dysprosium, erbium and yttrium, they are less likely to cause extensive oxygen ion displacement or vacancy ordering, which lead to conductivity decay and thus single dopants of these metal oxides are able to stabilize the fluorite structure of δ-Bi₂O₃.^{22–25} Jung *et al.* found that with two dopants, dysprosium and tungsten stabilized bismuth oxide achieved higher conductivity, again based on their ionic radii and dielectric polarizability.²⁶ Maria also reports that small amount of niobium oxide doped bismuth oxides yield a fluorite-type crystal structure.²⁷

In this study we explored how oxygen-ion conductivity in a metal oxide is related to the ignition temperature, by doping δ-Bi₂O₃. More specifically we evaluated the ignition behavior of seven doped Bi₂O₃ oxidized thermites which were chosen so as to enable systematic changes to their oxygen ion conductivity, without a change in crystal structure and morphology. Our results point to a critical oxygen ion conductivity of doped Bi₂O₃ that, when achieved through thermal activation, leads to an ignition condition.

Experimental

Sample preparation

Nano-aluminum particles (~50 nm) were purchased from Novacentrix Corporation, nano-sized carbon black (~50 nm) was obtained from Cabot Corporation and nano-tantalum powders (<50 nm) were purchased from Global Advanced Metals. Bi(NO₃)₃·5H₂O (≥98% pure), Y(NO₃)₃·6H₂O (99.8% pure) and NH₄NbO(C₂O₄)₂·xH₂O were purchased from Sigma-Aldrich. Dy(NO₃)₃·5H₂O (99.9% pure) and (NH₄)₆W₁₂O₃₉·xH₂O was purchased from Alfa Aesar. To dissolve Bi(NO₃)₃·5H₂O, 2 mol L⁻¹ nitric acid was used.

Seven different compositions with a constant dopant molar concentration of 15 mol% were investigated as listed in Table 1.

To ensure appropriate comparison, pure Bi₂O₃ is also synthesized. All compositions were prepared by aerosol spray pyrolysis²⁸ at 750 °C with a constant precursor concentration. Aerosol spray pyrolysis is a single droplet chemistry approach. So long as the temperature is substantially lower than the volatilization temperature of the individual metal components the resulting solid particle will have the same relative concentration as the original solution, insuring accurate stoichiometric fractions.

A 0.2 mol L⁻¹ precursor solution was atomized in a nebulizer into 1 μm droplets by compressed air flow. The atomized droplet flowed through a diffusion dryer, where most of the water was absorbed, and then decomposed into oxides in the furnace.

Table 1 Aerosol spray synthesized doped Bi₂O₃

Doped Bi ₂ O ₃ formula	Abbreviation
(Er ₂ O ₃) _{0.15} (Bi ₂ O ₃) _{0.85}	ESB
(Dy ₂ O ₃) _{0.15} (Bi ₂ O ₃) _{0.85}	DSB
(Y ₂ O ₃) _{0.15} (Bi ₂ O ₃) _{0.85}	YSB
(Dy ₂ O ₃) _{0.1} (W ₂ O ₆) _{0.05} (Bi ₂ O ₃) _{0.85}	DWSB10
(Dy ₂ O ₃) _{0.05} (W ₂ O ₆) _{0.1} (Bi ₂ O ₃) _{0.85}	DWSB5
(Dy ₂ O ₃) _{0.05} (Nb ₂ O ₅) _{0.1} (Bi ₂ O ₃) _{0.85}	DNSB
(W ₂ O ₆) _{0.15} (Bi ₂ O ₃) _{0.85}	WSB

The final product was collected in a Millipore membrane with a pore size of 0.4 micron.

To prepare the thermite composite, stoichiometric mixtures of nano-fuels (aluminum, carbon, or tantalum) and doped Bi_2O_3 were mixed and then sonicated in hexane for 30 min. While calculating the stoichiometry, the Al_2O_3 shell (19% of the mass) and Ta_2O_5 shell (30% of the mass) were considered. For the impedance measurement, each doped Bi_2O_3 sample was pressed into a 13 mm diameter pellet at 30 MPa with a thickness of ~ 1 mm. The pellets were subsequently sintered in air at 750°C for 16 h, and Engelhard gold paste was brushed onto both sides of the pellets. Platinum wires were attached to both sides of the painted pellet using gold paste and the cell were sintered at 500°C for 1 h to burn the organic additives from the paste.

Characterization

Crystal structure and morphology of doped Bi_2O_3 . The crystal structures of the synthesized Bi_2O_3 were characterized by X-ray diffraction (XRD) performed on a Bruker D8 diffractometer with $\text{Cu K}\alpha$ radiation. Le Bail refinement of all diffraction patterns was performed with the TOPAS 4.2 software.²⁹ The morphologies of the particles were measured by scanning electron microscopy (SEM) with a Hitachi SU-70. Size distributions were obtained by measuring 300 individual nanoparticles statistically from SEM images of each sample, using Nano Measurer 1.2 image analysis software.³⁰

T-Jump ignition test for thermite. Ignition temperature was measured in a temperature-jump/time-of flight mass spectrometer (T-Jump/TOFMS).³¹ The temperature of the wire was calculated from electric resistance based on Callendar–Van Dusen equation, using the data from simultaneously recorded applied voltage and current. Due to the small dimension of nanoparticles compared with the wire and based on our previous result, the temperature of the wire is essentially equal to the temperature of the thermite system.³²

Conductivity measurements. Oxygen ion conductivity was measured from the AC impedance analysis using a Solartron 1260 A, with a symmetric cell by two electrode electrochemical impedance spectroscopy over the frequency range of 1 Hz to 10^6 Hz with perturbation amplitude of 100 mV. The Solartron 1260 A was interfaced to a computer using the Zplot software for the data analysis. A nulling technique was used to remove any artifacts caused by inductive response of the test leads and the equipment to measure the small impedance at high temperature. The measurements were performed between 200 and 700°C or 200 and 750°C in air atmosphere with an interval of 50°C . The conductivities were converted from the bulk resistance and the dimensions of the sample based on $\sigma = L/RA$, where σ is the oxygen ion conductivity, R is the bulk resistance, L and A is the thickness and sectional area of the pellets.

Results and discussion

Structure and morphology

As the oxygen ion conductivity of Bi_2O_3 is highly dependent on crystal structure, it was important to ensure that all doped

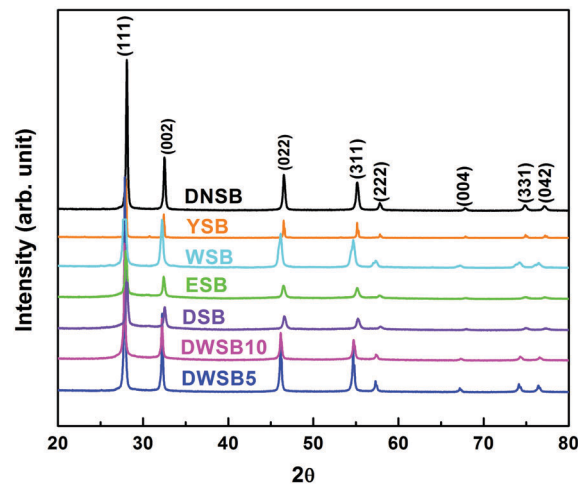


Fig. 1 X-ray diffraction patterns of aerosol spray synthesized doped Bi_2O_3 .

Bi_2O_3 samples had the same crystal structure. Fig. 1 shows XRD patterns for all seven doped Bi_2O_3 , showing that all doped Bi_2O_3 prepared were found to be pure fcc structure, indicating they are $\delta\text{-Bi}_2\text{O}_3$. The XRD pattern of pure Bi_2O_3 is shown in Fig. S1 (ESI[†]), showing a tetragonal structure, $\beta\text{-Bi}_2\text{O}_3$. Although $\alpha\text{-Bi}_2\text{O}_3$ is the only room-temperature stable structure, it was $\beta\text{-Bi}_2\text{O}_3$ that was obtained *via* aerosol spray pyrolysis, presumably because of the rapid quenching that occurs in aerosol pyrolysis processing that can result in meta-stable phases. The lattice parameters of seven $\delta\text{-Bi}_2\text{O}_3$ samples at room temperature were determined from the TOPAS program for calculating oxygen vacancy concentrations in Table 2. Since all doped Bi_2O_3 have the same crystal structure, it is reasonable to assume the crystal structure shouldn't have a controlling impact on ignition.

Fig. 2 shows the SEM images of DSB and DWBS5 as representative powders, indicating similar particle size distribution. SEM images of DSB at various magnifications can be found in Fig. S2 (ESI[†]). The diameter of the particles should be log-normally distributed corresponding to the original spray size distribution. As example we show the size distribution of DSB and DWBS5 and log-normal fit in Fig. S3 (ESI[†]). The log-normal fit parameters are listed in Table S1 (ESI[†]) and show that all particles have a similar narrow log-normal distribution with $\sigma = 0.453 \pm 0.003$, with an average diameter of ~ 100 nm. Since all particles have a similar size distribution and morphology we can reasonably remove these as variables.

Table 2 Calculated oxygen vacancy percentage in one unit cell and $[V_{\text{O}}^{\bullet\bullet}]$ of doped Bi_2O_3

Doped Bi_2O_3	Oxygen vacancy (%)	$[V_{\text{O}}^{\bullet\bullet}]$ ($\# \text{ cm}^{-3}$)
ESB	25	1.2×10^{22}
DSB	25	1.2×10^{22}
YSB	25	1.2×10^{22}
DWBS10	21.2	9.9×10^{21}
DNSB	20	9.6×10^{21}
DWBS5	17.5	8.1×10^{21}
WSB	13.7	6.3×10^{21}

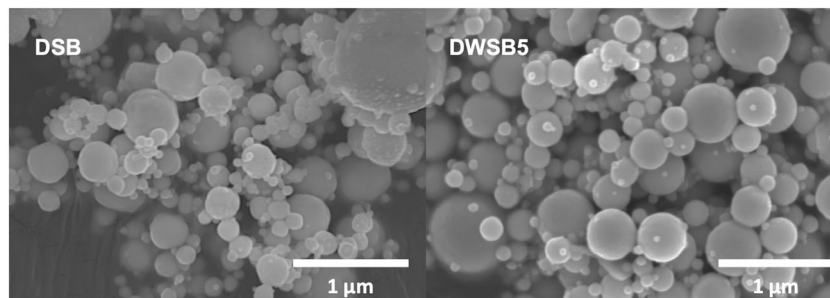


Fig. 2 SEM images of DSB and DWSB5 particles.

Oxygen ion conductivity

Fig. 3 shows typical impedance spectra obtained for WSB, as an example, at (a) 200 °C and (b) 500 °C. The assignment of a controlling mechanism for conductivity is based on the magnitudes of the measured capacitance as outlined in Table 1 of ref. 33. From this we determine that at low temperature ($T < 400$ °C), as Fig. 3a shows, the single semicircle at high frequency is attributed to the bulk properties of the sample, and the half semicircle at lower frequency attributed to the electrode impedance. At high temperature ($T \geq 400$ °C), as Fig. 3(b) shows, the high frequency semicircle corresponding to bulk resistance could no longer be seen, and the resistance was calculated from the intersection with the real axis at high frequency. Impedance spectra in Fig. 3 fitted in equivalent circuits and fitting parameters are shown in Fig. S4 (ESI†).

Fig. 4a shows an Arrhenius plot of the bulk ionic conductivity of doped Bi_2O_3 , showing, as expected, an increase in ion-conductivity with temperature. Since oxygen is the only mobile charge carrier in Bi_2O_3 , we can reasonably assign the bulk ionic conductivity to oxygen ion conductivity. The conductivities in the region of ignition temperature are shown with more detail in Fig. 4b. For doped Bi_2O_3 , it is found that the slope at high temperature ($T \geq 650$ °C) is smaller than at low temperature ($T < 650$ °C), indicating the activation energy change, due to an order-disorder transition of oxygen lattice in the material.^{24,25} Of the $\delta\text{-Bi}_2\text{O}_3$ samples, ESB and YSB showed the highest oxygen

ion conductivity, while WSB shows the lowest, which can be mainly attributed to differences in the oxygen vacancy concentration, $[V_{\text{O}}^{\bullet\bullet}]$ and metal-oxygen bond energy, since other microstructures of doped Bi_2O_3 are the same. $\delta\text{-Bi}_2\text{O}_3$ has a defect fluorite-type crystal structure (AX_2) in which 25% of the oxygen sites in the unit cell are vacant.³⁴ Er^{3+} , Y^{3+} have the same valence as Bi^{3+} , so it is reasonable to assume that ESB and YSB also have $\sim 25\%$ vacant oxygen sites in the unit cell. However, W^{6+} has a higher oxidation state, so WO_3 should correspondingly have $\sim 50\%$ more oxygen than AX_2 in the oxygen sites. Oxygen vacancy concentrations of ESB, WSB, DSB, YSB, DWSB5, DWSB10 and DNSB can thus be estimated based on the percentage of vacant oxygen sites in one unit cell, and the lattice parameter. The calculated oxygen vacancy percentage in one unit cell and $[V_{\text{O}}^{\bullet\bullet}]$ of those doped Bi_2O_3 are shown in Table 2. We also notice that the pure β phase Bi_2O_3 has a different conductivity trend compared with $\delta\text{-Bi}_2\text{O}_3$ samples, with an abrupt conductivity increase between 600 °C to 650 °C, which we attribute to a phase change from β to δ .³⁵

Ignition and oxygen ion conductivity

The reaction in the $\text{Al}/\text{Bi}_2\text{O}_3$ formulation is very violent, with an easily discernable visible ignition event. The measurements of ignition temperatures were repeated twice for each formulation and the results are listed in Table S2 (ESI†).

Based on the ignition temperature of $\text{Al}/\text{Bi}_2\text{O}_3$ and the measured conductivities for doped Bi_2O_3 , the oxygen ion conductivity at

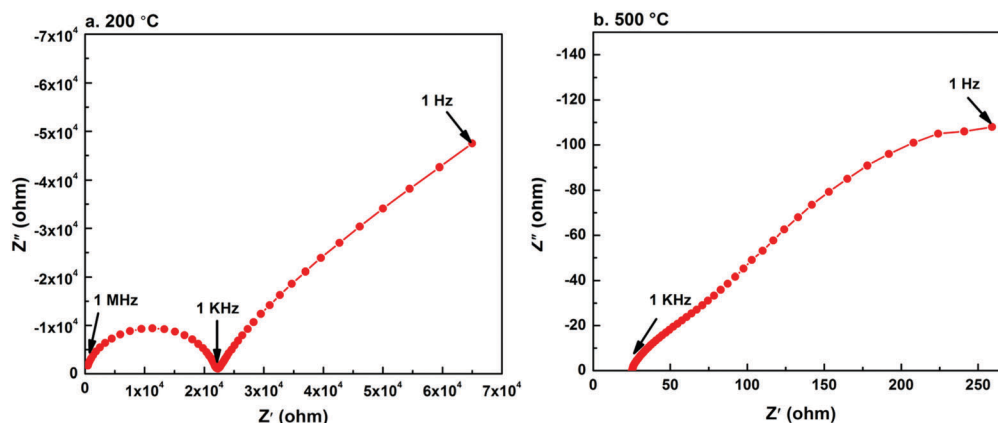


Fig. 3 Typical impedance spectra (in this case WSB) in air at: (a) 200 °C and (b) 500 °C.

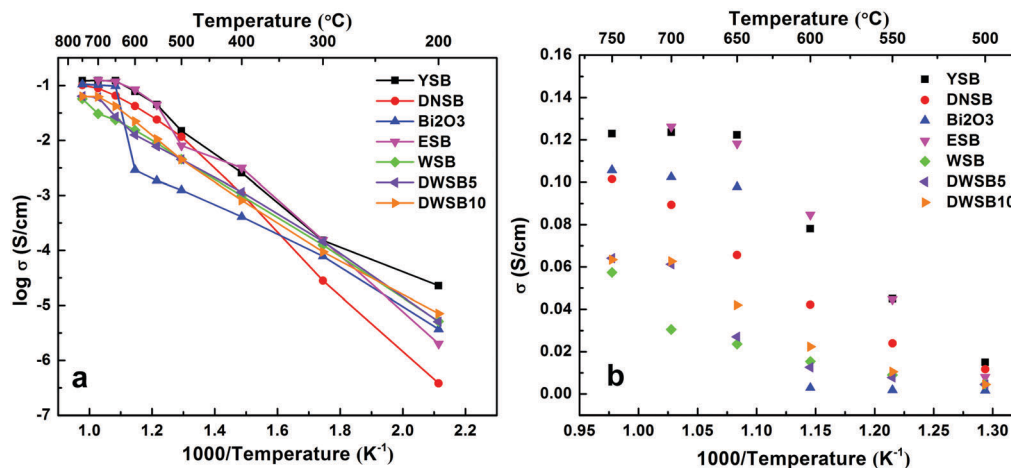


Fig. 4 (a) Arrhenius plot of measured ion-conductivities for doped Bi_2O_3 and pure Bi_2O_3 . (b) Zoomed in measured ion conductivities at 500–750 °C for doped Bi_2O_3 and pure Bi_2O_3 .

the point of ignition is shown in Fig. 5a. In Fig. 5a, we see four data points, corresponding to ESB, DSB, YSB and DNSB, with ignition slightly below the melting temperature of aluminum. These have higher conductivities at the ignition temperature than those that ignite above the melting temperature. The key feature of this plot is that ignition above the aluminum melting point, always occurs at the same oxygen ion conductivity.

Noting that ignition temperature is varying, but the oxygen ion conductivity at ignition is constant, even though conductivity is temperature sensitive as seen in Fig. 4, we may conclude that there exists a critical oxygen ion conductivity ($\sim 0.06 \text{ S cm}^{-1}$) that controls the ignition of $\text{Al}/\text{Bi}_2\text{O}_3$, when other parameters are held constant. WSB has the lowest oxygen ion conductivity, thus it reaches the critical conductivity at a higher temperature,

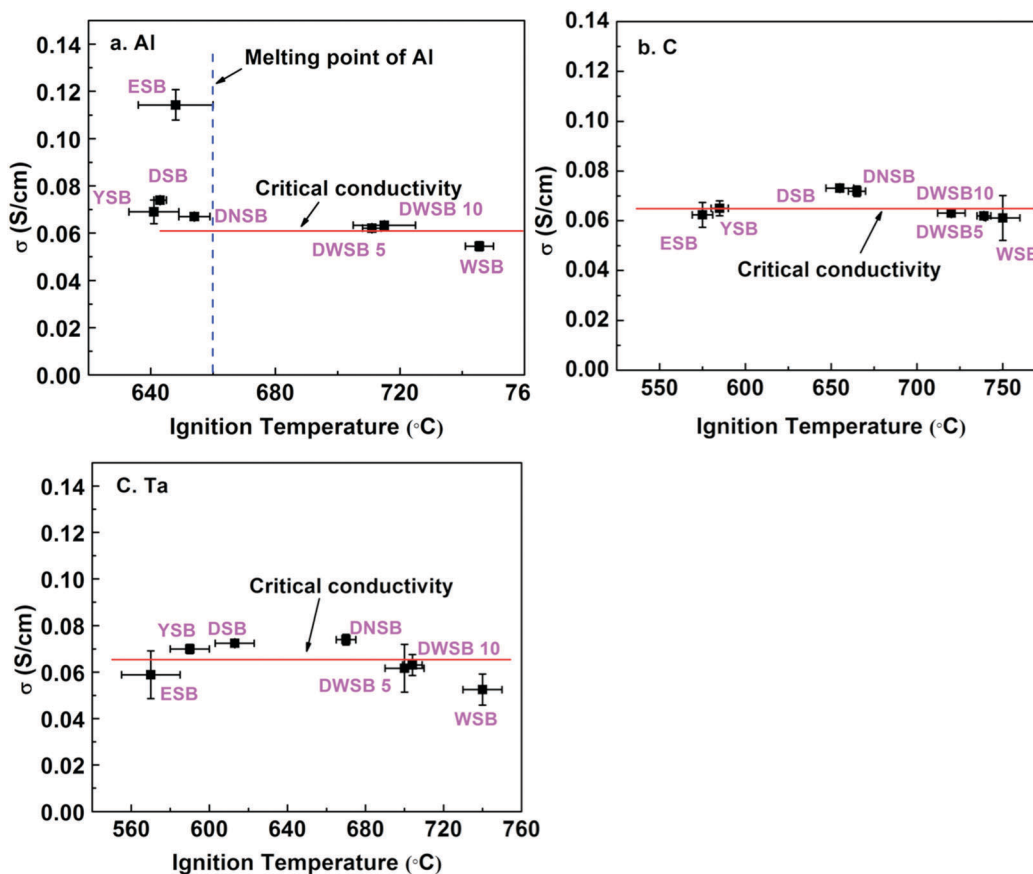


Fig. 5 Oxygen ion conductivity as a function of corresponding ignition temperature for (a) $\text{Al}/\text{doped Bi}_2\text{O}_3$, (b) $\text{C}/\text{doped Bi}_2\text{O}_3$ and (c) $\text{Ta}/\text{Bi}_2\text{O}_3$.

resulting a higher ignition temperature. Above the melting point, Al is the most mobile species, moving through the alumina shell faster than oxygen transport. Below the melting point it is possible that the reaction interface occurs within the oxide shell as has previously been discussed and requires higher oxygen ion mobility for ignition.

To further investigate the role of molten aluminum core, and the existence of a critical oxygen ion conductivity, we employed carbon as a fuel, which has no surface passivating oxide and no melting phase transition. In contrast to Al/Bi₂O₃, the C/Bi₂O₃ reaction is much less vigorous with no visible emission, thus for determining the point of ignition, temporal CO₂ release was used as shown in Fig. 6. The onset temperatures of five formulations are listed in Table S2 (ESI[†]). The oxygen ion conductivity as a function of corresponding reaction temperature is shown in Fig. 5b. Again we find ignition occurs at an oxygen ion conductivity $\sim 0.065 \text{ S cm}^{-1}$, indicating it is dominated by the oxygen ion transport of oxidizer, and the existence of a critical oxygen ion conductivity. It is interesting that C/Bi₂O₃ reaction occurs at a similar temperature as the ignition of Al/Bi₂O₃ as shown in Table S2 (ESI[†]).

Tantalum was also employed as a fuel to further compare with Al/Bi₂O₃ and C/Bi₂O₃. Similar to aluminum, tantalum also has a native oxide shell (Ta₂O₅), but has a very high melting point, with no melting phase transition in the ignition temperature regime. Tantalum is also a high energy density fuel, and the ignition of Ta/Bi₂O₃ was a discernable visible event that was recorded by high-speed camera. Results show that, again, Ta/Bi₂O₃ has similar ignition temperature (Table S2, ESI[†]) as Al/Bi₂O₃ and a critical oxygen ion conductivity of $\sim 0.065 \text{ S cm}^{-1}$ shown in Fig. 5c, indicating ignition is dominated by the oxygen ion transport of the oxidizer.

We note that three different fuels (Al, C and Ta) with very different physical-chemical properties are observed to have essentially equivalent critical oxygen ion conductivity for the ignition of doped Bi₂O₃ oxidized thermites. While this result is surprising, we should keep in mind that conductivity is a thermally activated process, and thus exponentially dependent on temperature, so that within a range of oxygen ion conductivity

ignition occurs. Ignition by its nature is essentially the point where the self-heating by exothermic reaction exceeds heat loss and a non-linear reaction event occurs. Thus the fact that a similar critical condition for initiation is found is perhaps not as surprising upon further reflection. It implies that since the heat loss terms are essentially equivalent for the three different metals that approximately the same flux of oxidizer is need to initiate non-linear heat release regardless of metal type. The different ignition temperatures just reflect when each particular oxidizer can achieve this critical condition.

We also measured the initiation temperatures of Al/ β -Bi₂O₃ and C/ β -Bi₂O₃. We found again that C/ β -Bi₂O₃ reaction starts at a similar temperature as the ignition temperature of Al/ β -Bi₂O₃ at $\sim 630 \text{ }^\circ\text{C}$, which lies exactly in the regime that oxygen ion conductivity increased abruptly from 0.002 S cm^{-1} to 0.97 S cm^{-1} from $600 \text{ }^\circ\text{C}$ to $650 \text{ }^\circ\text{C}$ and essentially where the critical conductivity lies.

Effect of oxygen vacancy concentration and bond energy on ignition temperature

Oxygen vacancies and oxygen ion mobility are integral to ion-conductivity based on eqn (1), where σ is the conductivity of oxygen ion, Zq is the charge of the ion (O^{2-} in this case), μ is the carrier mechanical mobility, and $[V_{\text{O}}^{\bullet\bullet}]$ is the oxygen vacancy concentration.

$$\sigma = Zq \cdot [V_{\text{O}}^{\bullet\bullet}] \cdot \mu \quad (1)$$

Previous research has found that μ depends on the activation energy of oxygen ion migration, which can be associated with average metal oxygen bond energy and the critical radius for oxygen ion transportation in the doped Bi₂O₃ lattice.³⁶ We thus turn our attention to how $[V_{\text{O}}^{\bullet\bullet}]$ and average metal-oxide bond energy affects the ignition temperature as we did in our previous study of perovskites.¹⁵ For fluorite type doped δ -Bi₂O₃ in which that cation is 6-coordinated with oxygen anions, the average metal-oxide bond energy is calculated based on eqn (2) where $\Delta H_{\text{A}_m\text{O}_n}$ is the heat of formation of A_mO_n at 298 K, ΔH_{A} is the heat of sublimation of A-metal at 298 K and D_{O_2} is the dissociation energy of gaseous oxygen.¹⁸

$$\Delta(\text{A} - \text{O}) = \frac{1}{6m} \left(\Delta H_{\text{A}_m\text{O}_n} - m\Delta H_{\text{A}} - \frac{n}{2} D_{\text{O}_2} \right) \quad (2)$$

Presumably, higher $[V_{\text{O}}^{\bullet\bullet}]$ and lower bond energy should lead to higher oxygen ion conductivity, thus it follows that materials with the high $[V_{\text{O}}^{\bullet\bullet}]$ and low bond energy would have lower ignition temperatures. Fig. 7 clearly shows that this is indeed the case, as ignition temperature decreases with $[V_{\text{O}}^{\bullet\bullet}]$ (Fig. 7a) while increasing with bond energy (Fig. 7b). For instance, in Fig. 7a, the $[V_{\text{O}}^{\bullet\bullet}]$ of ESB and DSB are the largest, resulting in ESB and DSB having the lowest ignition temperatures. In comparison, WSB has the smallest $[V_{\text{O}}^{\bullet\bullet}]$, resulting in the highest ignition temperature. Boyapati *et al.*¹⁴ found that oxygen ion transport relies on interstitial migration, which is dependent on the occupancy of interstitial sites. W^{6+} has a higher oxidation state, thus WSB has more oxygen ions occupying the

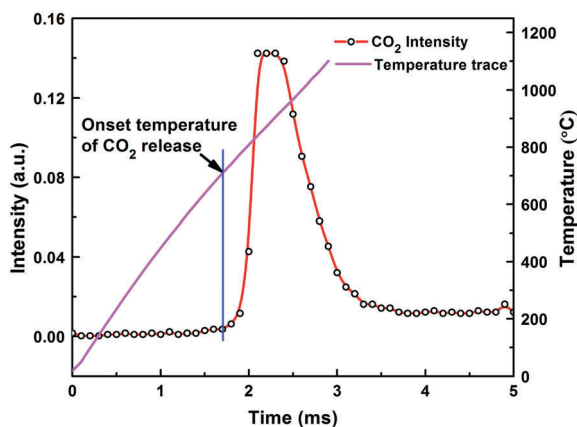


Fig. 6 Representative T-Jump/TOFMS plot showing the temporal CO₂ release from C/DWSB5.

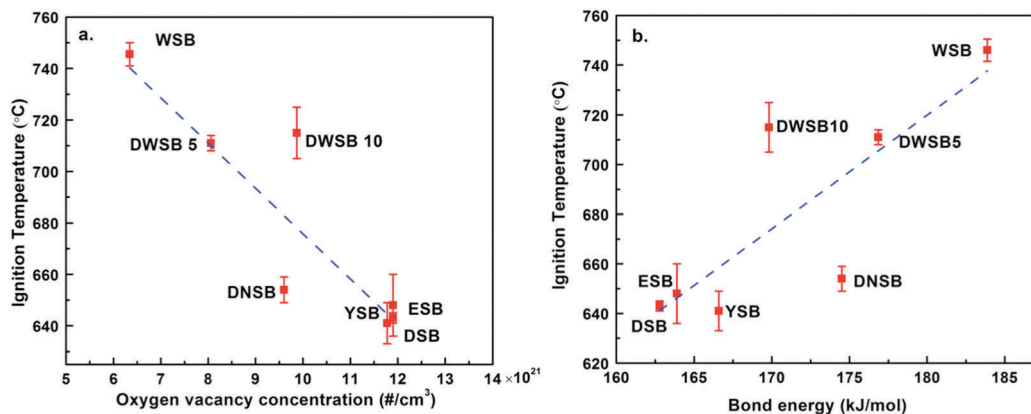


Fig. 7 The (a) oxygen vacancy concentrations and (b) bond energy vs. their corresponding ignition temperatures of seven Al/doped Bi₂O₃ formulations.

interstitial sites, resulting in even lower oxygen ion conductivity. In Fig. 7b, ESB and DSB have smaller bond energies, resulting in lower temperature. These results imply in a general sense that it may be possible to introduce oxygen vacancies in an oxidizer to achieve high oxygen ion conductivity, and tune ignition behavior.

Ignition and oxygen ion diffusivity

Oxygen ion's electric mobility is related to mechanical mobility, and in turn through the Nernst–Einstein relation, can be related to diffusivity. Thus from eqn (3) the measured conductivity is directly proportional to the diffusivity D , where k is Boltzmann's constant.³⁷

$$\sigma = Z^2 q^2 \cdot [V_{\text{O}}^{\bullet\bullet}] \cdot D/k \cdot T \quad (3)$$

We have previously shown the oxygen vacancy concentration in Table 2. At our very high heating rates, we can expect that the defect density $[V_{\text{O}}^{\bullet\bullet}]$ is probably relatively constant until the point of ignition. Thus from the measured oxygen ion conductivities at different temperatures shown in Fig. 4, and known vacancy concentration, we can from eqn (3) deduce the oxygen ion diffusivity as a function of temperature, which is presented as an Arrhenius plot in Fig. S5 (ESI[†]).

Diffusivity has an exponential temperature dependence nominally expressed by eqn (4)³⁸ where D_0 is temperature-independent pre-exponential, Q_d is the activation energy for diffusion and R is the gas constant.

$$D = D_0 \cdot \exp\left(-\frac{Q_d}{RT}\right) \quad (4)$$

Q_d can be estimated from the slope of the Arrhenius plot of oxygen ion diffusivity (Fig. S5, ESI[†]) and leads to an activation energy for diffusion between 70–100 kJ mol⁻¹. We can also measure the activation energy of ignition using Flynn–Wall–Ozawa iso-conversion method^{39,40} from eqn (5), where β is the heating rate, T is the ignition temperature and E_a is the activation energy for ignition. The ignition temperatures at different heating rates (1.3×10^5 to 5.5×10^5 °C s⁻¹) were measured with the T-Jump/TOFMS. Results show that the activation energy for ignition of Al/DWSB 5 is $\sim 86 \pm 7$ kJ mol⁻¹ (shown in Fig. S6, ESI[†]), which is

similar to the activation energy for diffusion, implying that the ignition for condensed phase reaction is consistent with an oxygen ion transport controlled mechanism and consistent with the concept of a critical ion-conductivity for ignition as shown in Fig. 5.

$$\ln \beta = \text{const.} - \frac{1.052E_a}{RT} \quad (5)$$

Based on the ignition temperature, and the Arrhenius plot of diffusivities of doped Bi₂O₃ at different temperature, the diffusivity as a function of corresponding ignition temperature for Al/Bi₂O₃, C/Bi₂O₃, and Ta/Bi₂O₃ are shown in Fig. 8.

These results show that there exists a trend that the ignition of doped Bi₂O₃ with aluminum, carbon and tantalum, respectively, increased with oxygen ion diffusivity from ESB to WSB, so long as aluminum is melted. This is mainly a result of decreased $[V_{\text{O}}^{\bullet\bullet}]$ from ESB to WSB shown in Table 2. For example, WSB has the lowest $[V_{\text{O}}^{\bullet\bullet}]$, thus in order to reach the critical metric for ignition, the oxygen ion diffusivity of WSB must reach a higher level so as to achieve sufficient oxygen ion flux to initiate ignition.

The characteristic diffusion time, $t = (0.75r)^2/D$,³⁸ based on a 100 nm diameter particle and an average diffusivity ($\sim 10^{-6}$ cm² s⁻¹), is $\sim 1.4 \times 10^{-5}$ s and is quite close to the measured pressure rise time $\sim 1.0 \times 10^{-5}$ s of Al/Bi₂O₃ obtained in pressure cell measurements (Fig. S7, ESI[†]).⁴¹ This could imply that the initial fast reaction observed in pressure cells is controlled by the diffusion of oxygen from the oxidizer.

We (Zhou *et al.*⁴²) recently reported on a critical reaction rate for Al ignition, which is invariant of ignition temperature and heating rate. Employing a similar method (in ESI[†]) to calculate the reaction rate at the ignition point of Al/Bi₂O₃, yields a value of $(1.24 \pm 0.17) \times 10^{-1}$ mol m⁻² s⁻¹, which is consistent with Zhou *et al.*'s assumption that reaction rate is roughly constant. The average reaction rate, R , of a Bi₂O₃ particle with an Al particle could be estimated based on the burning time, t ($\sim 2 \times 10^{-4}$ s), measured from the optical signal obtained in pressure cell measurements (Fig. S7, ESI[†]) and the dimensions of the Bi₂O₃ particle in eqn (6):

$$R = \frac{n_{\text{Bi}_2\text{O}_3}}{s_{\text{Bi}_2\text{O}_3} \cdot t} = \frac{4\pi r^3 \rho_{\text{Bi}_2\text{O}_3}}{4\pi r^2 M_{\text{Bi}_2\text{O}_3} t} \quad (6)$$

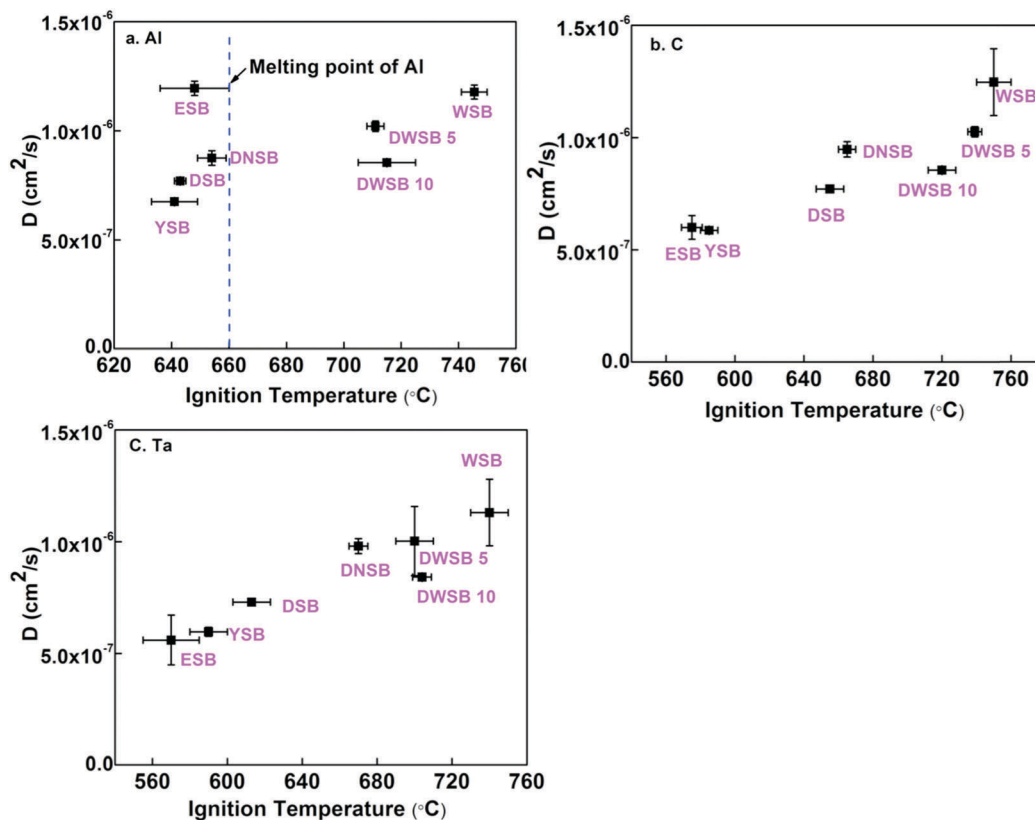


Fig. 8 Oxygen ion diffusivity as a function of corresponding ignition temperature for (a) Al/doped Bi_2O_3 , (b) C/doped Bi_2O_3 and (c) Ta/ Bi_2O_3 .

Herein, $n_{\text{Bi}_2\text{O}_3}$ is the molecular number of Bi_2O_3 molecules in a Bi_2O_3 particle, $S_{\text{Bi}_2\text{O}_3}$ is the surface area of a Bi_2O_3 particle, r is the radius of a Bi_2O_3 particle (~ 50 nm), $\rho_{\text{Bi}_2\text{O}_3}$ is the density of Bi_2O_3 (~ 9.00 g cm^{-3}), and $M_{\text{Bi}_2\text{O}_3}$ is the molar mass of Bi_2O_3 (465.96 g mol^{-1}). Eqn (6) leads to an average reaction rate, R , over the whole burning time, of ~ 1.6 mol m^{-2} s^{-1} . This implies that the diffusion controlled ignition rate is about one order of magnitude smaller than the observed average reaction rate, and consistent with a self-accelerating process.

Conclusions

In this study, we investigated the existence of a correlation between oxygen ion transport in doped Bi_2O_3 , and the ignition temperature. By measuring the ionic conductivities as a function of temperature of seven doped Bi_2O_3 's with the same crystal structure and morphology, and their corresponding ignition temperatures with three fuels (Al, C, Ta) respectively, we found a critical oxygen ion conductivity exists for Bi_2O_3 oxidized thermite ignition as long as aluminum is molten. The activation energy for ignition of Al/ Bi_2O_3 is close to the activation energy of oxygen ion diffusion, which is consistent with an oxygen transport limited rate. Finally we find a correlation between the oxygen vacancy concentration and bond energy vs. ignition temperature. The latter suggests that we can consider the possibility of manipulating microscopic properties within

a crystal, in order to tune the resultant energetic properties, *i.e.* in this case ignition temperature.

Acknowledgements

This work was made possible through support of the Army Research Office and the Defense Threat Reduction Agency. We also gratefully acknowledge the support of experimental facility from Dr Eric Wachsman's group at the University of Maryland's Energy Research Center.

References

- 1 S. H. Fischer and M. C. Grubelich, *Theoretical Energy Release of Thermites, Intermetallics, and Combustible Metals*, 24th International Pyrotechnics Seminar, Monterey, Ca, July, 1998.
- 2 E. L. Dreizin, Metal-Based Reactive Nanomaterials, *Prog. Energy Combust. Sci.*, 2009, 35(2), 141–167.
- 3 N. H. Yen and L. Y. Wang, Reactive Metals in Explosives, *Propellants, Explos., Pyrotech.*, 2012, 37, 143–145.
- 4 F. Noor, H. Zhang, T. Korakianitis and D. Wen, Oxidation and Ignition of Aluminum Nanomaterials, *Phys. Chem. Chem. Phys.*, 2013, 15(46), 20176–20188.
- 5 V. Rosenband, Thermo-Mechanical Aspects of the Heterogeneous Ignition of Metals, *Combust. Flame*, 2004, 137(3), 366–375.

- 6 M. A. Trunov, M. Schoenitz and E. L. Dreizin, Effect of Polymorphic Phase Transformations in Alumina Layer on Ignition of Aluminium Particles, *Combust. Theory Modell.*, 2006, **10**(4), 603–623.
- 7 K. T. Sullivan, W. A. Chiou, R. Fiore and M. R. Zachariah, *In Situ* Microscopy of Rapidly Heated Nano-Al and Nano-Al/WO₃ Thermites, *Appl. Phys. Lett.*, 2010, **97**(13), 133104.
- 8 K. T. Sullivan, N. W. Piekielek, C. Wu, S. T. Chowdhury, S. T. Kelly, T. C. Hufnagel, K. Fezzaa and M. R. Zachariah, Reactive Sintering: An Important Component in the Combustion of Nanocomposite Thermites, *Combust. Flame*, 2012, **159**(1), 2–15.
- 9 W. Zhou, J. B. DeLisio, X. Wang and M. R. Zachariah, Reaction Mechanisms of Potassium Oxysalts Based Energetic Composites, *Combust. Flame*, 2017, **177**, 1–9.
- 10 M. Schoenitz, S. M. Umbrajkar and E. L. Dreizin, Kinetic Analysis of Thermite Reactions in Al-MoO₃ Nanocomposites, *J. Propul. Power*, 2007, **23**(4), 683–687.
- 11 T. Bazyn, N. Glumac, H. Krier, T. S. Ward, M. Schoenitz and E. L. Dreizin, Reflected Shock Ignition and Combustion of Aluminum and Nanocomposite Thermite Powders, *Combust. Sci. Technol.*, 2007, **179**(3), 457–476.
- 12 G. Jian, S. Chowdhury, K. Sullivan and M. R. Zachariah, Nanothermite Reactions: Is Gas Phase Oxygen Generation From the Oxygen Carrier an Essential Prerequisite to Ignition?, *Combust. Flame*, 2013, **160**(2), 432–437.
- 13 N. W. Piekielek, L. Zhou, K. T. Sullivan, S. Chowdhury, G. C. Egan and M. R. Zachariah, Initiation and Reaction in Al/B₂O₃ Nanothermites: Evidence for the Predominance of Condensed Phase Chemistry, *Combust. Sci. Technol.*, 2014, **186**(9), 1209–1224.
- 14 S. Boyapati, E. D. Wachsman and N. Jiang, Effect of Oxygen Sublattice Ordering on Interstitial Transport Mechanism and Conductivity Activation Energies in Phase-Stabilized Cubic Bismuth Oxides, *Solid State Ionics*, 2001, **140**(1), 149–160.
- 15 X. Wang, T. Wu and M. R. Zachariah, Doped Perovskites to Evaluate the Relationship Between Fuel-Oxidizer Thermite Ignition and Bond Energy, Electronegativity and Oxygen Vacancy, *J. Phys. Chem. C*, 2017, **121**(1), 147–152.
- 16 M. Barsoum, *Fundamentals of Ceramics*, McGraw-Hill Companies, Inc., USA, 1997.
- 17 F. S. Baumann, J. Fleig, H. U. Habermeier and J. Maier, Ba_{0.5}Sr_{0.5}Co_{0.8}Fe_{0.2}O_{3-δ} Thin Film Microelectrodes Investigated by Impedance Spectroscopy, *Solid State Ionics*, 2006, **177**(35), 3187–3191.
- 18 D. R. Lide, Standard Thermodynamic Properties of Chemical Substances, *CRC handbook of Chemistry and Physics*, 2007, vol. 5.
- 19 L. Malter and D. B. Langmuir, Resistance, Emissivities and Melting Point of Tantalum, *Phys. Rev.*, 1939, **55**(8), 743.
- 20 D. W. Jung, K. Duncan and E. D. Wachsman, Doubly Doped Bi₂O₃ Electrolytes with Higher Conductivity, *ECS Trans.*, 2006, **1**(7), 63–71.
- 21 T. Takahashi, H. Iwahara and Y. Nagai, High Oxide Ion Conduction in Sintered Bi₂O₃ Containing SrO, CaO or La₂O₃, *J. Appl. Electrochem.*, 1972, **2**(2), 97–104.
- 22 E. D. Wachsman, S. Boyapati and N. Jiang, Effect of Dopant Polarizability on Oxygen Sublattice Order in Phase-Stabilized Cubic Bismuth Oxides, *Ionics*, 2001, **7**(1–2), 1–6.
- 23 T. Takahashi and H. Iwahara, High Oxide Ion Conduction in Sintered Oxides of the System Bi₂O₃-WO₃, *J. Appl. Electrochem.*, 1973, **3**(1), 65–72.
- 24 M. J. Verkerk and A. J. Burggraaf, High Oxygen Ion Conduction in Sintered Oxides of the Bi₂O₃-Dy₂O₃ System, *J. Appl. Electrochem.*, 1981, **128**(1), 75–82.
- 25 E. D. Wachsman and K. T. Lee, Lowering the Temperature of Solid Oxide Fuel Cells, *Science*, 2011, **334**(6058), 935–939.
- 26 D. W. Jung, K. L. Duncan and E. D. Wachsman, Effect of Total Dopant Concentration and Dopant Ratio on Conductivity of (DyO_{1.5})_x-(WO₃)_y-(BiO_{1.5})_{1-x-y}, *Acta Mater.*, 2010, **58**(2), 355–363.
- 27 M. Thompson, *Synthesis and Characterisation of δ-Bi₂O₃ Related Materials Stabilised by Substitutions of Ca, Ga, Nb and Re*, University of Birmingham, 2010.
- 28 T. Wu, A. SyBing, X. Wang and M. R. Zachariah, Aerosol Synthesis of Phase Pure Iodine/Iodic Biocide Microparticles, *J. Mater. Res.*, 2017, **32**(4), 890–896.
- 29 R. W. Cheary and A. A. Coelho, Fundamental Parameters Approach to X-Ray Line-Profile Fitting, *J. Appl. Crystallogr.*, 1992, **25**, 109–121.
- 30 Y. He, F. Wu, X. Sun, R. Li, Y. Guo, C. Li, L. Zhang, F. Xing, W. Wang and J. Gao, Factors That Affect Pickering Emulsions Stabilized by Graphene Oxide, *ACS Appl. Mater. Interfaces*, 2013, **5**(11), 4843–4855.
- 31 L. Zhou, N. Piekielek, S. Chowdhury and M. R. Zachariah, T-Jump/Time-of-Flight Mass Spectrometry for Time-Resolved Analysis of Energetic Materials, *Rapid Commun. Mass Spectrom.*, 2009, **23**, 194–202.
- 32 C. Snehaunshu, K. Sullivan, N. Piekielek, L. Zhou and M. R. Zachariah, Diffusive vs. Explosive Reaction at the Nanoscale, *J. Phys. Chem. C*, 2010, **114**(20), 9191–9195.
- 33 J. T. Irvine, D. C. Sinclair and A. R. West, Electroceramics: Characterization by Impedance Spectroscopy, *Adv. Mater.*, 1990, **2**(3), 132–138.
- 34 H. A. Harwig, On the Structure of Bismuthsesquioxide: The α, β, γ, and δ-Phase, *Z. Anorg. Allg. Chem.*, 1978, **444**(1), 151–166.
- 35 N. M. Sammes, G. A. Tompsett, H. Näfe and F. Aldinger, Bismuth Based Oxide Electrolytes-Structure and Ionic Conductivity, *J. Eur. Ceram. Soc.*, 1999, **19**(10), 1801–1826.
- 36 H. Zhao, N. Xu, Y. Cheng, W. Wei, N. Chen, W. Ding, X. Lu and F. Li, Investigation of Mixed Conductor BaCo_{0.7}Fe_{0.3-x}Y_xO_{3-δ} with High Oxygen Permeability, *J. Phys. Chem. C*, 2010, **114**(41), 17975–17981.
- 37 H. Rickert, *Electrochemistry of solids*, Springer Verlag, Berlin, 1982.
- 38 W. D. Kingery, H. K. Bowen and D. R. Uhlmann, *Introduction to ceramics*, John Wiley & Sons, New York, 1976.
- 39 J. H. Flynn and L. A. Wall, General Treatment of the Thermogravimetry of Polymers, *J. Res. Natl. Bur. Stand.*, 1966, **70**(6), 487–523.

- 40 G. Jian, L. Zhou, N. W. Piekielek and M. R. Zachariah, Low Effective Activation Energies for Oxygen Release from Metal Oxides: Evidence for Mass-Transfer Limits at High Heating Rates, *ChemPhysChem*, 2014, **15**(8), 1666–1672.
- 41 H. Wang, G. Jian, W. Zhou, J. B. DeLisio, V. Lee and M. R. Zachariah, Metal Iodate-Based Energetic Composites and Their Combustion and Biocidal Performance, *ACS Appl. Mater. Interfaces*, 2015, **7**(31), 17363–17370.
- 42 W. Zhou, J. B. DeLisio, X. Wang, G. C. Egan and M. R. Zachariah, Evaluating Free Vs Bound Oxygen On Ignition Of Nano-Aluminum Based Energetics Leads to A Critical Reaction Rate Criterion, *J. Appl. Phys.*, 2015, **118**(11), 114303.